Infrared Studies of the SO_2 Clathrate Hydrate

Zhenfeng Zhang[†] and George E. Ewing*

Department of Chemistry, Indiana University, Bloomington, Indiana 47405

Received: October 7, 2003; In Final Form: December 19, 2003

Using infrared spectroscopy, transitions among ice, solution, and clathrate phases are compared with the predictions of the SO_2-H_2O phase diagram in the temperature range −20 to 10 °C and SO_2 pressures from 50 to 900 mbar. The infrared signatures of clathrate and ice, as well as SO_2 in a variety of phases are recorded and interpreted in terms of their environments. The consequences of SO_2 in confined geometries within ice are explored.

Introduction

Previous studies of the SO_2 clathrate hydrate have provided methods for its synthesis,[1−5] its phase diagram,[1−3,6−8] crystal structure,[9] and the infrared features of SO_2 in the hydrate at cryogenic temperatures.[10] The first report of the SO_2 hydrate was published in 1829,[4] and its crystal structure was determined by M. V. Stackelberg and H. R. Muller.[9] The clathrate host of SO_2 (and other gas molecules[6]) is termed an S-1 type consisting of six tetrakaidecahedral (14-sided) and two smaller dodecahedral (12-sided) cages formed by 46 water molecules in a cubic unit cell. The occupancy of the cages depends on the temperature and pressure.[5] It was found that 97% of the large cages and 25% of the small cages were occupied at 0 °C and at an SO_2 pressure of 0.327 bar.[5] Infrared spectra of the hydrate at −180 °C provided resolved band centers that allowed the SO_2 molecules to be distinguished in the large and small cages.[10] The SO_2 hydrate has been prepared with water vapor and SO_2 gas where the nucleation for the hydrate formation is achieved by using dry ice to chill the walls of the container.[5] At cryogenic temperatures, hydrate formation is more difficult and requires the presence of other molecules or clathrates to facilitate the nucleation.[10] The primary motivation for our study is the infrared characterization of both the SO_2 guest and its clathrate host near the ice melting point (−20 to 6 °C) and the study of the clathrate formation from supercooled SO_2 solutions. To this end we utilize attenuated total reflection (ATR) spectroscopy on a face of a cooled germanium prism on which films of water solutions, ice, and hydrates are prepared for investigation.

Methods and Materials

Photometry. The SO_2-H_2O system is investigated by attenuated total reflection (ATR) spectroscopy, a method reviewed extensively elsewhere.[11−13] In our experiments infrared radiation travels from the substrate, a germanium prism, toward vacuum (or more exactly low-pressure vapor) and is reflected at the interface. When the incident angle is greater than the critical angle, which is 14° for germanium,[13] total internal reflection occurs. However electromagnetic radiation extends beyond the substrate as an evanescent wave that is attenuated by absorbing material (e.g., the SO_2-H_2O system) at the interface.

* Author to whom correspondence should be addressed. E-mail: ewingg@indiana.edu.

[†] Present address: Department of Chemistry, University of California, Irvine, CA.

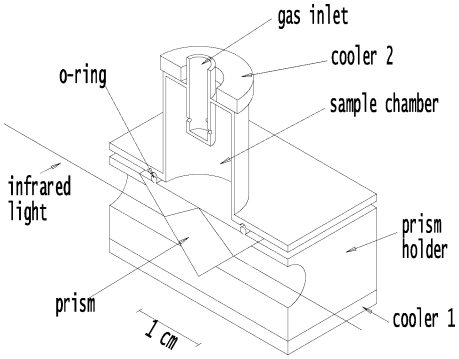

Figure 1. The optical cell. Films of water are grown on the upper face of a germanium prism. The prism is cooled by Peltier thermoelectric elements coolers 1 and 2. Water cooling tubes for the Peltier elements are not shown. Samples of H_2O and/or SO_2 are introduced as vapor through the gas inlet of the sample chamber. The film is investigated by infrared light. The optical cell is enclosed in a vacuum dewar (not shown).

We define the optical response as extinction, $E = \log I_0/I$, where I_0 is proportional to the optical throughput at the substrate/vacuum interface and I is the response with the film.

In practice, the films we shall study are of the order of 1 μm which exceeds the typical penetration depth of 0.3 μm of our optical arrangement.[13] The extinction is a sensitive function of the incident angle. For example, the extinction at 3400 cm^{-1} varies by 25% as the incident angle changes from 50° to 60°.[13] Thus while band centers and band profiles are relatively invariant to the 10° incident angle changes, the shift in extinction values compromises photometry measurements. Consequently, due to the uncertainty in the incident angle we use, 55 ± 5°, which includes the angles spanned by the cone of light into the ATR prism, we are unable to extract accurate optical cross sections.

The Optical Cell. The optical cell and clathrate hydrate generator is a temperature-controlled vacuum assembly. The inner part of this assembly is the ATR prism mount shown in Figure 1. A stainless steel cylinder, serving as the sample chamber of volume 4 cm^3, is attached through an O-ring to the base of a 45°−90°−45° germanium prism (Harrick Scientific, Ossining, NY). Polyethylene−propylene O-rings (American Seal, Houston, TX), which are resistant to aqueous SO_2, are used for sealing purposes. The prism sits in a copper holder. The prism holder and the sample chamber are separately cooled

10.1021/jp037019j CCC: $27.50
Published on Web 02/13/2004

with Peltier thermoelectric elements (Melcor, Trenton, NJ), cooler 1 and cooler 2. A thermistor for the temperature controller (Wavelength Electronics, Bozeman, MT) is glued with thermal epoxy (Melcor, Trenton, NJ) to the prism holder at a position that is next to the cold surfaces of the Peltier element. Similarly, another thermistor is attached to the sample chamber. The thermistors, not shown in Figure 1, were calibrated at 0.0 °C with a mixture of ice and water.

The optical cell is mounted in an aluminum vacuum chamber not shown in Figure 1. The vacuum chamber has two 3′ wedged ZnSe windows (Infrared Optical Products, S. Farmingdale, NY), which prevent fringes in infrared spectra as the light comes into and out of the cell. The incoming radiation from the FTIR is refracted at the vacuum/prism interface at the left to make an incident angle of about 55° at the base surface of the prism. Electric conduits, tubes for evacuation, sample introduction to the gas inlet, and cooling water for the Peltier elements are fed through the bottom plate of the vacuum chamber. A stainless dewar (Cole-Parmer) is mounted to the top of the vacuum chamber to cryopump residual water vapor with liquid nitrogen. A turbo molecular pump (Turbovac 151, Leybold, Germany) and rotary vane pump (S5E, Leybold, Germany) are used to maintain a vacuum of 10^{-6} mbar.

Making Films. Prior to an experiment, the germanium prism was cleaned for 30 min in a solution of 90% water + 5% (30% H_2O_2) + 5% (30% NH_4OH).[14−16] Then it was rinsed with distilled water. After the prism was allowed to dry in the air, the hydrate generator was assembled. To prepare an SO_2 aqueous solution, the prism temperature was lowered with cooler 1 to a desired temperature. Then, water vapor was admitted to the sample chamber to form a water film on the cold germanium prism. Condensation was monitored from spectrum change. Next, SO_2 gas was introduced into the sample chamber to a desired pressure. After that, cooler 2 was turned on to reduce the temperature gradient across the base surface of the prism. Liquid films of SO_2 were prepared by condensing the vapor at 640 mbar onto the prism at −20 °C.

Spectrophotometric water (John Matthy, Ward Hill, MA), after being treated with several freeze−pump−thaw cycles, was used as the water vapor source. Anhydrous SO_2 gas, 99.9% (Air Products and Chemicals, Allentown, PA), was used without further purification. The pressure of the system was monitored with a Baratron 122A with a PDR-C-2C power supply and readout (MKS Instruments Inc., Andover, MA) and an ion gauge (Kurt J. Lesker Co., Clairton, PA) with gauge controller 260 (Granville-Philips).

Spectroscopy. Infrared spectra were taken with a Nicolet Magna 550 spectrometer (Madison, WI) equipped with an MCT (mercury−cadmium−telluride) detector. Resolution was set at 4 cm^{-1}. Triangle apodization and zero filling were used to process the spectra. The sample compartment of the spectrometer was purged with a Balston 75-62 FTIR Purge Gas Generator (Haverhill, MA) to reduce water vapor and CO_2 gas from the optical path.

Overview

We shall be studying the interaction of SO_2 with water near ambient conditions, by that we mean temperatures from −20 °C to 10 °C and at pressures near or below 1 bar. To provide preparation for discussion of our experiments, we present a portion of the SO_2−H_2O phase diagram that spans the thermodynamic conditions of our measurements. We also survey the nature of aqueous SO_2 solutions.

Phase Diagram. The relevant part of the phase diagram of the SO_2−H_2O system is regenerated from previous experiments[1−3]

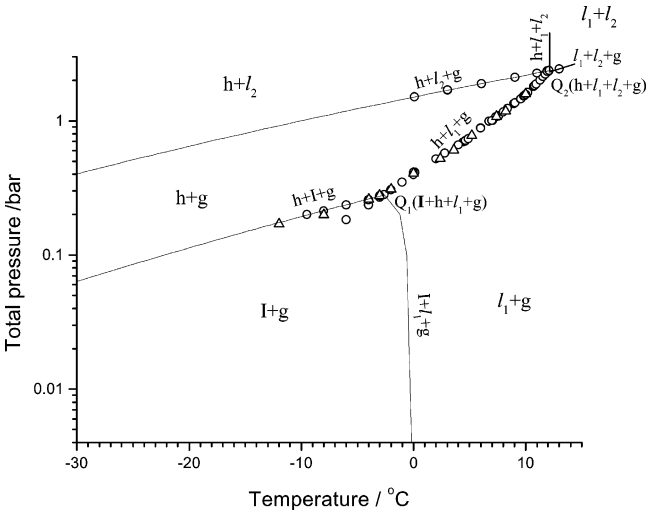

Figure 2. Phase diagram of the SO_2−H_2O system. Data points are taken from papers of Roozeboom (o)[1,2] and Tammann and Keige (Δ).[3] Extrapolations of the h+⅓+g and h+**I**+g lines and construction of the **I**+⅓+g line are discussed in the text.

and shown in Figure 2. H. W. Bakhuis Roozeboom obtained the phase diagram of the SO_2−water system by measuring dissociation pressures of the hydrate at various temperatures.[1,2] Later on, part of the phase diagram was either repeated or expanded.[3] The diagram is divided into five two-phase bivariant zones by six triple-phase univariant lines. The h+**I**+g, h+⅓+g and **I**+⅓+g lines are in the lower part of the diagram and the h+⅓+g, h+⅓+⅔, and ⅓+⅔+g lines in the upper part. Here h is hydrate, **I** is ice, ⅓ is a saturated SO_2 aqueous solution, ⅔ is liquid SO_2 saturated with water, g is a mixture of SO_2 gas and H_2O vapor. The h+**I**+g, h+⅓+g, and h+⅓+⅔ lines form the boundary of hydrate formation, with bivariant h+g, h+⅓ zones on one side, and **I**+g, ⅓+g, and ⅓+⅔ zones on the other. The univariant lines come together at two invariant quadruple points, Q_1(h+**I**+g+⅓) at (−2.6 °C, 0.247 bar) and Q_2(h+⅓+⅔+g) at (12.1 °C, 2.36 bar).

The **I**+⅓+g line is drawn qualitatively using as one point the melting point of ice, 0 °C, with its partial pressure 6 mbar.[17] For higher pressures, on introduction of SO_2 vapor, we make use of the freezing point depression of ice, ΔT, in the presence of a dilute solute,

$$\Delta T = K_f b \tag{1}$$

with $K_f = 1.86$ K/(mol kg^{-1}), the cryoscopic constant of water, and b the SO_2 molality.[18] With $b = 0.6$ m at $p = 0.2$ bar SO_2 near 0 °C, from Henry's Law[19] we find $\Delta T = 1.2$ K. The coexistence line is then −1.2 °C at 0.2 bar and likewise −0.6 °C at 0.1 bar. Using these estimated points, the **I**+⅓+g line is constructed in Figure 2.

To have guidance for this work at temperatures below −12 °C for the h+**I**+g line and below 0 °C for the h+⅓+g line, where experimental data are not available, the data are extrapolated to −30 °C using the Clausius−Clapeyron equation,[18]

$$\frac{d \ln p}{dT} = \frac{\Delta H}{RT^2} \tag{2}$$

where p is the total pressure (essentially the pressure of SO_2 since the partial pressure of water vapor is so low in this region of the phase diagram), and R is the gas constant. The values of ΔH for either the dissociation enthalpy of the hydrate into ice

and gas across the h+**I**+g line, or the enthalpy of evaporation of the SO_2 solution across the h+⁄2+g line, was obtained by fitting the available data to eq 2. The extrapolations are shown in the SO_2-H_2O phase diagram of Figure 2.

Aqueous SO_2. The two reactions that concern us are

$$SO_2(g) \overset{H}{\rightleftharpoons} SO_2(aq) \tag{3}$$

and

$$SO_2(aq) + H_2O \overset{K}{\rightleftharpoons} H^+ + HSO_3^- \tag{4}$$

Reaction 3 expresses the gas solubility as quantified by Henry's law constant $H = [SO_2(aq)]/p_{SO_2}$. The dissociation of solvated SO_2 into bisulfite is given by reaction 4 with equilibrium constant K. (Further dissociation into sulfite, $SO_3^=$, is negligible for the conditions of our experiments.) Measurements of H and K by Johnstone and Leppla[19] span the temperature range from 50 °C to 0 °C. We have extrapolated their results to −30 °C.

To understand the conditions of one of our experiments we consider, as an example, the nature of a SO_2 water solution at −10 °C. Here extrapolation finds $H = 5.0$ mol kg^{-1} bar^{-1} and $K = 0.030$ mol kg^{-1}. At a pressure of 900 mbar SO_2, this corresponds to a molar concentration of 4.5 m. The relative concentration of bisulfite to dissolved SO_2, obtained from eqs 3 and 4, is given by

$$[HSO_3^-]/[SO_2(aq)] = (K/H_{pSO_2})^{1/2} \tag{5}$$

(In our discussions of concentrations we assume that the activity coefficients of the species are unity.) This ratio is 0.08 at 900 mbar so that the solution is mostly (93%) solvated SO_2 at −10 °C. However conditions considered in the uptake by the water component of ice or snow by trace amounts of atmospheric SO_2, where $p_{SO_2}$is typically 10^{-6} bar,[20−30] the calculated ratio is 80. In these cases the dissolved sulfur oxides are essentially all (99%) HSO_3^-.

Measurements and Discussions

In our experiments, the SO_2 hydrate has been formed from supercooled SO_2 aqueous solutions.

We began by preparing a thick film of supercooled water at −10 °C as presented in Figure 3a. The water is characterized by its overlapping OH stretching modes, ν_1 and ν_3, which have an absorption centered at 3400 cm^{-1}. The bending mode, ν_2, band is at 1643 cm^{-1}, librational mode, ν_L, at 667 cm^{-1}, and the combination band, $\nu_2 + \nu_L$, at 2143 cm^{-1} as assigned by others.[31,32]

Then SO_2 gas was introduced gradually to a final pressure of 900 mbar into the sample chamber. Two features at 1332 and 1151 cm^{-1} grow in. These features are those previously identified as the ν_3 and ν_1 vibrations of aqueous SO_2,[33] and are accompanied by weaker absorptions at 3620, 1200, and 1050 cm^{-1} due to bisulfite ions and marked with asterisks. When the final pressure was reached after 10 min, no growth in spectroscopic features could be detected, establishing that the SO_2 solution was saturated. This final spectrum is shown in Figure 3b. From the SO_2-H_2O phase diagram, Figure 2, it can be seen that the thermodynamically stable state at −10 °C, 900 mbar is (h+g), i.e., the coexistence of the hydrate and SO_2 gas. Therefore the SO_2 solution represented in Figure 3b is non-equilibrium, i.e., supercooled.

Thirty minutes after the introduction of the gas, both the band positions and bandwidths of the SO_2 features began to change.

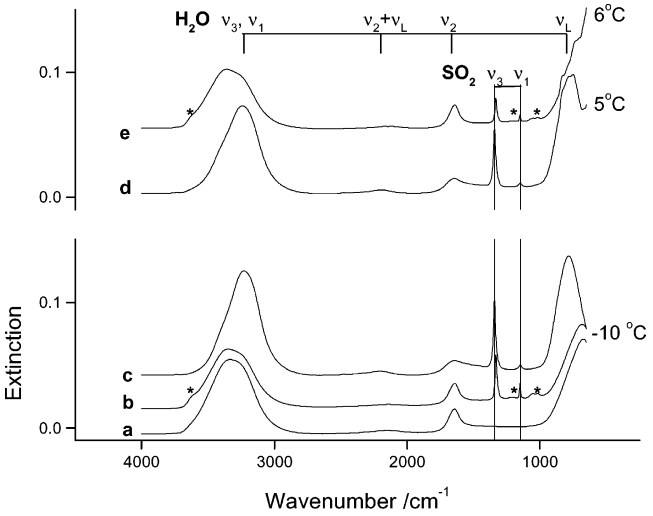

Figure 3. The SO_2−hydrate from concentrated aqueous solution. *Lower panel, formation of hydrate*: (a) Thick film water at −10 °C. (b) Supersaturated solution at −10 °C and 900 mbar. (c) SO_2 hydrate at −10 °C and 885 mbar. *Upper panel, melting of hydrate*. (d) SO_2 hydrate at 5 °C. (e) SO_2 solution at 6 °C. The asterisks indicate bisulfite ions. The vertical lines indicate the band centers of SO_2 adsorptions in the hydrate.

TABLE 1: Absorption Bands of SO_2

	band center (bandwidth)/cm^{-1}			
assignment	SO_2(aq)[a]	SO_2(l)[b]	SO_2(h)[c]	SO_2(g)[d]
ν_2	526	523		518
ν_1	1151(9)	1146(11)	1149(25)	1151
ν_3	1332(17)	1330(17)	1342(20)	1362
$\nu_3 + \nu_1$	2470(15)	2488(15)	2476(13)	2500

[a] SO_2(aq): supercooled water solution (−10 °C, 885 mbar). [b] SO_2(l): neat liquid (−20 °C, 640 mbar). [c] SO_2(h): clathrate hydrate (−10 °C, 885 mbar). [d] SO_2(g): gas (20 °C, 30 mbar).

This was accompanied by profile alteration of the H_2O bands as well. After 24 h (the pressure had dropped to 885 mbar) there were no noticeable changes in the H_2O band profiles or the ν_1 and ν_3 SO_2 features. Moreover the bisulfite features, signatures for the presence of aqueous SO_2 through reaction 4,[33] could no longer be detected. This final spectrum, which we take to be the SO_2−hydrate is shown in Figure 3c.

The gradual formation of the hydrate from the saturated (supercooled) water solution is likely limited in part by the diffusion of dissolved SO_2. The saturated solution at 4.5 m corresponds to a mole ratio SO_2/H_2O of 1:12. The hydrate with large and small cages filled requires the ratio SO_2/H_2O of 1:5.75.[34] (The more practical mole ratio limit with the cages partially filled is somewhat higher.[35]) The necessary SO_2 enrichment therefore requires adsorption of the gas-phase molecules onto the liquid interface and diffusion onto the cage-building sites of the hydrate.

The absorptions of liquid-state SO_2 and its aqueous solutions can be fitted to Lorentzian functions. By contrast, while the ν_3 mode of SO_2 in the hydrate is Lorentzian, the ν_1 mode with its sharpened band center is distinctly non-Lorentzian. The results of the profile analysis are also given in Table 1. The band centers and bandwidths will become the diagnostic for the SO_2 environment. The SO_2 spectra in the various environments are compared in Figure 4.

The assignment of the features in Figure 3c to SO_2−hydrate can be further confirmed by comparing its melting point with that given by the phase diagram, Figure 2, on crossing the h+⁄1+g line from the (h+g) zone to the (⁄1+g) zone. Spectra

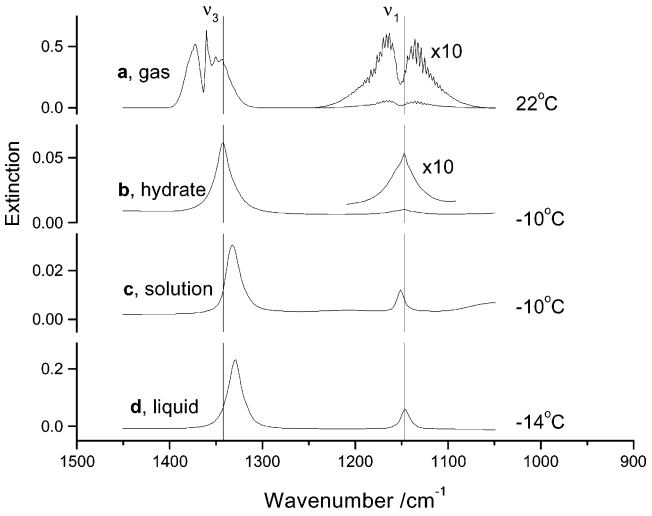

Figure 4. Infrared spectra of SO_2 in different states. (a) SO_2 gas in a 12.5 cm long cell at (22 °C, 30 mbar). (b) SO_2 hydrate at (−10 °C, 885 mbar). (c) SO_2 (supercooled) solution at (−10 °C, 900 mbar). (d) SO_2 liquid at (−20 °C, 640 mbar). The line denotes band centers of SO_2 in the hydrate. (a) Transmission spectrum. (b**)** (c), (d), ATR spectra.

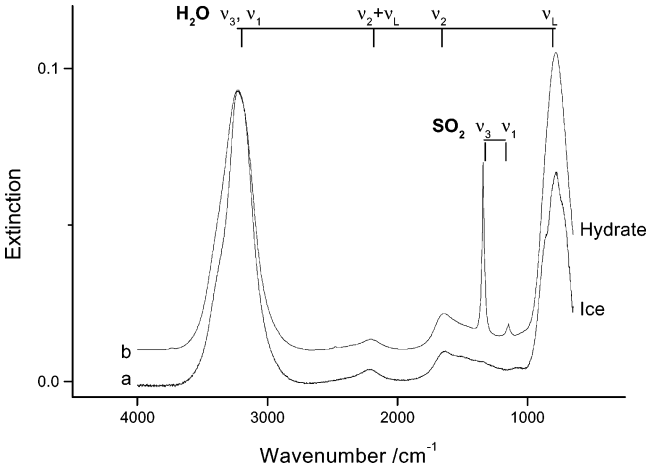

Figure 5. Spectra of ice at −7 °C (a), and spectra of SO_2 hydrate (−10 °C, 885 mbar) (b**)**.

in Figures 3d and 3e were taken during warming of the hydrate during which the pressure remains essentially constant at 885 mbar. The lack of change of the spectra at −10 and 5 °C with time suggests that the hydrate was at equilibrium with the gas at both temperatures. It can be seen that the ν_3 and ν_1 SO_2 bands retain their positions and profiles up to 5 °C, but shift to 1332 and 1151 cm^{-1} at 6 °C, the same frequencies as those of the solution in Figure 3b or the table. This transition from hydrate to solution is in good agreement with the phase diagram.

Comparison of spectra of the SO_2 clathrate hydrate, Figure 5b, and ice taken at −7 °C, Figure 5a, shows that absorption profiles of H_2O molecules in both ice and the clathrate hydrate resemble each other, yet exhibit subtle differences. That there are no measurable 1050 or 1151 or 1332 cm^{-1} absorptions, markers for bisulfite, suggesting that the SO_2 solution has transformed to the clathrate hydrate completely, and is therefore pure. Figure 5b shows infrared bands of H_2O molecules in the SO_2 clathrate hydrate, in essential agreement with those recorded by Bertie and Othen[36] using other guest molecules. The band centers of the OH stretching vibrations, ν_3 and ν_1, of ice and clathrate hydrate are the same (3240 ± 20 cm^{-1}), but the profiles differ. The bandwidth of ice is 270 ± 20 cm^{-1}, while that of the clathrate is 290 ± 20 cm^{-1}.

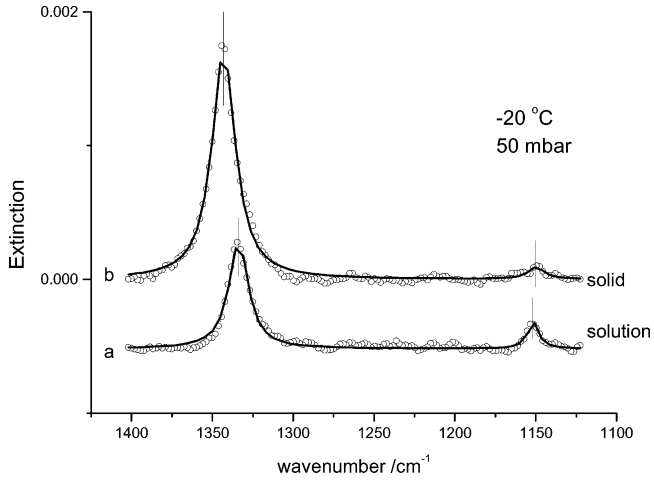

Figure 6. The SO_2 hydrate from dilute aqueous solution. (a) SO_2 solution at −20 °C and 50 mbar. (b) SO_2 hydrate in an ice matrix at −20 °C and 50 mb. Open circles are experimental data. The solid lines are fitted with Lorentzian equations.

The next experiment was undertaken with a dilute solution prepared at −20 °C using 50 mbar of SO_2. With $H = 8.5$, we find $[SO_2(aq)] = 0.42$ m or a concentration an order of magnitude lower than that previously used. The spectrum of this solution is given in Figure 6a. The band position (bandwidth) of the ν_3 SO_2 feature is 1334(14) cm^{-1}, and when compared with Figure 4c and the table (accepting an error limit of ±2 cm^{-1}) clearly confirm this to be an aqueous solution. The ν_1 feature at 1152(8) cm^{-1} is also in agreement with the assignment to $SO_2(aq)$.

The band positions of water features (not shown) also support the assignment to the liquid. Inspection of the phase diagram on Figure 2 shows that the equilibrium conditions of this system indicate ice and vapor (**I**+g) as the phases. The system must therefore be a supercooled solution.

Five minutes after solution preparation, freezing spontaneously occurred. This is made evident by the disappearance of the characteristic liquid water band at 3400 cm^{-1} in the OH stretching region (not shown) and the appearance of the solid (ice or hydrate) feature near 3200 cm^{-1}. The ν_3 signature of SO_2 in Figure 6b has now become 1343(17) cm^{-1}. The coincidence of the ν_3 band profile with Figure 4b and the table clearly indicate that SO_2 hydrate has formed. The feature near 1150 cm^{-1}, whose weakness does not permit a bandwidth determination, is consistent with its assignment to ν_1 of SO_2. However closer examination of the OH stretching region reveals a band center of 3210 cm^{-1} and bandwidth 270 cm^{-1} characterizing ice and not clathrate (compare Figures 5a and 5b). The spectroscopic assignments are then consistent with a heterogeneous solid-principally ice with a small fraction of SO_2− clathrate. (No time-dependent measurements were taken but presumably equilibrium, into gas and ice phases, would have been established after a sufficiently long wait.)

According to the phase diagram, a pressure of about 100 mbar is required for clathrate formation at −20 °C. The necessary increase in pressure from 50 mbar could have been achieved by the expulsion during ice formation of SO_2 into surrounding solution pockets thereby increasing local concentrations sufficiently to allow clathrate production. This is a natural consequence of ice being notoriously intolerant of impurities.[35] In studies of the photochemistry of chlorobenzene in ice at −20 °C, Klán et al.[37] observed anomalies that are consistent with aggregation of molecules on freezing of very dilute solutions. Similarly dilute aqueous solutions of H_2SO_4 or NaCl are

believed to be expelled into grain boundaries on freezing, enhancing the formation of liquid containing nodes and veins.[38] These types of aggregations of water in confining geometries may be similar to those we propose for the dilute SO_2 solutions on freezing.

Spectroscopic Signatures. We extract now the information contained in the spectroscopic profiles of SO_2 and H_2O in the experiments we have presented.

We consider first the SO_2 spectra summarized on Figure 4 and in the table. The ν_1 and ν_3 absorption in the various states can be easily distinguished from each other and contain information on the different environments of the molecule.

The gas phase spectrum in Figure 4a, taken under low resolution conditions, reveals partially resolved vibration−rotation envelopes in the ν_1 and ν_3 regions that span 50 to 100 cm^{-1}.

The spectrum of SO_2 in solution, Figure 4c, and in the liquid state, Figure 4d, although quantitatively distinguishable, are remarkably similar and bear little relationship to the gas-phase features. Their spectroscopic profiles, well modeled by Lorentzian functions, are characterized by their band centers and bandwidths in the table. Both the band shape and the order of magnitude value of the bandwidth, $\sim$10 cm^{-1}, are consistent with spectra of many molecules in their liquid environments.[39]

Turning now to the SO_2 hydrate, Figure 4b, we find an anomaly in the ν_1 feature. It is distinctly non-Lorentzian with a sharpening at the band center and a suggestion of shoulders on either side. The bandwidth is more than double that of SO_2 in the neat liquid or solution states. This spectroscopic signature suggests that the SO_2 molecule in the hydrate is gaslike. The SO_2 molecule is approximately a prolate symmetric rotor and so exhibits type A and type B vibration−rotation bands.[40] The symmetric stretching vibration, ν_1, for the gas-phase molecule, is associated with rotation about the C_2 axis and gives rise to P and R branches. In the hydrate the interaction of the SO_2 with the confining walls of the clathrate cage results in its rotation being slightly hindered. As a consequence, the manifold of the vibration−rotation energy levels are altered. One effect of this sort of perturbation on the vibration−rotation envelope is to induce a Q-branch.[41] There is then a closer resemblance of the ν_1 SO_2 hydrate profile to the gas-phase spectrum than to that of the solution or neat liquid. The ν_3 profile of the hydrate however does not bear an obvious relation to the gas-phase absorption. One can rationalize this observation by noting that for this vibration the accompanying rotation is about the axis perpendicular to the molecular plane giving rise to A-type P, Q, and R branches. This rotation sweeps out a greater volume than that of the B type, and its manifold of levels is more greatly perturbed.

In addition to the SO_2 infrared features in the hydrate being different from those in other states, they are also somewhat dissimilar to those at cryogenic temperatures. Fleyfel et al.[10] observed a doublet in the ν_3 region at 1347 and 1342 cm^{-1} which they associated with vibration of the SO_2 molecules in, respectively, small and large cages of the clathrate. The temperature of their measurements, −180 °C, resulted in narrow bandwidths which allowed them to resolve the small doublet splitting. Our bandwidth of $\sim$20 cm^{-1} obscures this 5 cm^{-1} splitting. We note that SO_2 occupancy of the large cages is favored in both experiments and our determination of 1342 cm^{-1} is in agreement with the −180 °C large cage result. Finally the broader bandwidth we have observed at −10 °C, over those at −180 °C, is consistent with the increased population of higher hindered rotor states of SO_2 molecules in the clathrate cages.

While quantitative information on the extinctions of the SO_2 bands in the various environments is not available, some qualitative comparisons are useful. The peak extinctions of SO_2 in the solution and liquid states show that their values in the liquid state are an order of magnitude greater for both ν_3 and ν_1 features. This can be rationalized, in part, by the higher SO_2 molecular density in the neat liquid over the 4.5 m solutions. The peak extinction ratio of ν_3 to ν_1 is roughly 3:1 for both the solution and the neat liquid. By contrast this extinction ratio is about 10:1 for both the clathrate hydrate and gas-phase spectra. In part, the relative weakness of the peak extinction of the ν_1 band in both the clathrate hydrate and gas phase is due to the broad bandwidths. This is a consequence of the extensive B-type rotational manifolds of the free rotor in the gas phase and its slightly hindered motion in the clathrate hydrate.

The spectroscopic signatures of the H_2O vibrations of the clathrate hydrate have been compared to that of ice in Figure 5. The band centers of the observed vibrational fundamentals ν_1, ν_2, ν_3, the librational mode, ν_L, and the combination band $\nu_2+\nu_L$ of the hydrate and ice agree to within experimental uncertainties. Here we have adopted the assignments for ice given by Petrenko and Whitworth.[42] The only distinguishing features between the two states are the profiles and more specifically the bandwidths of the ν_1 and ν_3 fundamental bands. It is significant that it is in this region, involving the OH stretching vibrations, that the absorption is most sensitive to the nature of the hydrogen bonding networks.[31,32] Band centers, bandwidths, and oscillator strengths undergo significant changes among the gas, liquid, and ice phases. In particular, the band centers shift from 3700 cm^{-1} to 3400 cm^{-1}, to 3200 cm^{-1} in going from the non-hydrogen bonding, i.e., dangling hydrogen,[43] to liquid water,[31,32] to ice,[31,32] respectively. Indeed there is a convincing correlation between the strength of the hydrogen bond and the shift of the OH stretching vibration band center.[32] The identity of the band centers for ice and the hydrate therefore suggests that the hydrogen bond strength is essentially the same in both states. This is consistent with an enthalpy change of only 1 kJ/mol in the transformation from I_h ice to the (empty) type S-1 clathrate cage.[6] But in ice, the environment of all water molecules is essentially the same except that each can occupy one of six orientations.[31,42] By contrast in the clathrate hydrate, a water molecule (in addition to its orientational possibilities) may share different numbers of five- and six-membered rings that comprise the 14- or 12-sided clathrate cages. This would account for the broader clathrate hydrate bandwidth. Other work using the HDO and D_2O isotopes in clathrate hydrates to explore the nature of bonding in the cages from infrared signatures has also been published.[44,45]

Conclusions

Pure SO_2 clathrate hydrate was made from aqueous supercooled solutions. The infrared spectrum of the clathrate hydrate has a characteristic profile. The H_2O bands of the hydrate resemble those of ice but with subtle band-shape differences that reflect their differing hydrogen bonding networks. The SO_2 absorptions of the hydrate differ from those in other phases as well as from that of the hydrate at cryogenic temperatures. It is suggested that the SO_2 molecules in the clathrate hydrate are gaslike. The clathrate hydrate forms from a dilute SO_2 aqueous solution under conditions not in accord with the phase diagram. It is suggested that on freezing the solution, SO_2 is expelled into small confining geometries that give rise to high enough pressures to permit the clathrate hydrate formation.

Acknowledgment. This work was supported by the National Science Foundation through Grant NSF CHE-9816299.

References and Notes

(1) Roozeboom, H. W. B. *Recl. Trav. Chim. Pays-Bas* **1884**, *3*, 29.
(2) Roozeboom, H. W. B. *Recl. Trav. Chim. Pays-Bas* **1885**, *4*, 67.
(3) Tammann, G.; Krige, G. J. R. *Z. Anorg. Allg. Chem.* **1925**, *146*, 179.
(4) Rive, A. D. L. *Ann. Chim. Phys Ser.* **1829**, *2* (40), 401.
(5) Cady, G. H. *J. Phys. Chem.* **1983**, *87*, 4437; *J. Chem. Educ.* 1873, *60*, 915.
(6) Davidson, D. W. *Water: A Comprehensive Treatise*; Plenum Press: New York, 1973; Vol. 2, p 115.
(7) Findlay, A. *The Phase Rule and Its Applications*, 2nd ed.; Longmans, Green and Co.: London, 1906.
(8) Gmelin, J. F. *Handbuch der an organischem Chemie, Schwefel*, 8th ed.; Verlag Chemie: Weinheim, 1960; Vol. B, No. 2.
(9) Stakelberg, M. V.; Mulleer, H. R. *Z. Elektrochem.* **1954**, *58*, 25.
(10) Fleyfel, F.; Richardson, H. H.; Devlin, J. P. *J. Phys. Chem.* **1990**, *94*, 7032.
(11) Harrick, N. S. *Internal Reflection Spectroscopy*; Wiley: New York, 1967.
(12) Zhang, Z.; Ewing, G. E. *Anal. Chem.* **2002**, *74*, 2578.
(13) Zhang, Z. Ph.D. Dissertation, Indiana University, 2002.
(14) Kern, W. *RCA ENG* **1983**, *28*, 99.
(15) Riegler, H.; Engel, M. *Ber. Bunsen-Ges.-Phys. Chem. Chem. Phys.* **1991**, *95*, 1424.
(16) Herminghaus, S.; Jacobs, K.; Mecke, K.; Bischof, J.; Fery, A.; Ibn-Elhaj, M.; Schlagowski, S. *Science* **1998**, *282*, 916.
(17) *Smithsonian Meteorological Tables 1951*, 6th ed.; Smithsonian Institution, Washington, DC, 1951.
(18) Atkins, P. *Physical Chemistry*, 6th ed.; Freeman: New York, 1997.
(19) Johnstone, H. F.; Leppla, P. W. *J. Am. Chem. Soc.* **1934**, *56*, 2233.
(20) Sommerfeld, R. A.; Lamb, D. *Geophys. Res. Lett.* **1986**, *13*, 349.
(21) Valdez, M. P.; Bales, R. C.; Stanley, D. A.; Dawson, G. A. *J. Geophys. Res.* **1987**, *92* (D8), 9779.
(22) Valdez, M. P.; Bales, R. C.; Dawson, G. A. *J. Geophys. Res.* **1987**, *92* (D8), 9789.
(23) Clapsaddle, C.; Lamb, D. *Geophys. Res. Lett.* **1989**, *16*, 1173.
(24) Valdez, M. P.; Dawson, G. A.; Bales, R. C. *J. Geophys. Res.* **1993**, *94* (D9), 1685.
(25) Conklin, M. H.; Bales, R. C. *J. Geophys. Res.* **1993**, *98* (D9), 16851.
(26) Conklin, M. H.; Sommerfeld, R. A.; Laird, S. K.; Villinski, J. E. *Atmos. Environ.* **1993**, *A27*, 159.
(27) Choi, J.; Conklin, M. H.; Bales, R. C.; Sommerfeld, R. A. *Atmos. Environ.* **2000**, *34*, 793.
(28) Chu, L.; Diao, G. W.; Chu, L. T. *J. Phys. Chem. A* **2000**, *104*, 7565.
(29) Clegg, S. M.; Abbatt, J. P. D. *J. Phys. Chem. A* **2001**, *105*, 6630.
(30) Huthwelker, T.; Lamb, D.; Baker, M.; Swanson, B.; Peter, T. *J. Colloid Interface Sci.* **2001**, *238*, 147.
(31) Eisenberg, D. S.; Kauzmann, W. *The Structure and Properties of Water*; Oxford University Press: New York, 1969.
(32) Pimentel, G. C.; McClelland, A. L. *The Hydrogen Bond*; Reinhold: New York, 1960.
(33) Zhang, Z.; Ewing, G. E. *Spectrochim. Acta A* **2002**, *582*, 2105.
(34) von Stackelburg, M. *Naturwissenschaften* **1949**, *36*, 327.
(35) Gross, G. W.; Svec, R. K. *J. Phys. Chem. B* **1997**, *101*, 6282.
(36) Bertie, J. E.; Othen, D. A. *Can. J. Chem.* **1973**, *51*, 1159.
(37) Klán, P.; Ansorgová, A.; Favero, D. D.; Holoubek, I. *Tetrahedron Lett.* **2000**, *41*, 7785.
(38) Mader, H. J. Glaciology **1992**, *38*, 359.
(39) *The Aldrich Library of FT-IR Spectra*, Vol. 1; Pouchert, C. J., Ed.; Aldrich Chemical Co. Inc., Milwaukee, WI, 1985.
(40) Shelton, R.; Fletcher, W. *J. Chem. Phys.* **1953**, *21*, 2178.
(41) Ewing, G. E. *J. Chem. Phys.* **1962**, *37*, 2250.
(42) Petrenko, V. F.; Whitworth, R. W. *Physics of Ice*; Oxford University Press: Oxford, 1999.
(43) We take this to be the mean of the ν_1 and ν_3 band centers of gas-phase H_2O.
(44) Fleyfel, F.; Devlin, J. P. *J. Phys. Chem.* **1988**, *92*, 631.
(45) Richardson, H. H.; Wooldridge, P. J.; Devlin, J. P. *J. Chem. Phys.* **1985**, *83*, 4387.